ISSN 0021-3640, JETP Letters, 2020, Vol. 111, No. 10, pp. 568–574. © Pleiades Publishing, Inc., 2020.
Published in Russian in Pis'ma v Zhurnal Eksperimental'noi i Teoreticheskoi Fiziki, 2020, Vol. 111, No. 10, pp. 674–681.

CONDENSED MATTER

Formation of the ω Phase in the Titanium–Iron System under Shear Deformation

B. B. Straumal[a, b, c, d, *], A. R. Kilmametov[b, d], A. A. Mazilkin[a, d], A. S. Gornakova[a], O. B. Fabrichnaya[e], M. J. Kriegel[e], D. Rafaja[e], M. F. Bulatov[f], A. N. Nekrasov[g], and B. Baretzky[d]

[a] *Institute of Solid State Physics, Russian Academy of Sciences, Chernogolovka, Moscow region, 142432 Russia*
[b] *Chernogolovka Center of Russian Academy of Sciences, Chernogolovka, Moscow region, 142432 Russia*
[c] *National University of Science and Technology MISiS, Moscow, 119049 Russia*
[d] *Institute of Nanotechnology, Karlsruhe Institute of Technology, Eggenstein-Leopoldshafen, 76344 Germany*
[e] *TU Bergakademie Freiberg, Institute of Materials Science, Freiberg, 09599 Germany*
[f] *Scientific and Technological Center of Unique Instrumentation, Russian Academy of Sciences, Moscow, 117342 Russia*
[g] *Institute of Experimental Mineralogy, Russian Academy of Sciences, Chernogolovka, Moscow region, 142432 Russia*
**e-mail: straumal@issp.ac.ru*

Received April 11, 2020; revised April 15, 2020; accepted April 15, 2020

The effect of the phase composition on the α/β-Ti(Fe) → ω-Ti(Fe) transformation in the Ti–4 wt % Fe alloy under shear strain with high-pressure torsion (HPT) has been studied. For shear deformation by means of HPT, two initial states of the alloy were used, which significantly differed in the morphology of the phases and the concentration of iron atoms in the β phase. During HPT, a stationary state occurred in both sample series, which is characterized by the presence of a single ω phase containing 4 wt % Fe and by a grain size of about 200 nm. Thus, the HPT state is equifinal and independent of the initial phase composition of the samples. It was found that under the influence of HPT in Ti–4 wt % Fe alloys not only martensitic (shear) transformation into the ω phase occurs, but also a significant mass transfer of atoms of the alloying element. An analysis of the change in the torsion torque directly in the HPT process made it possible to estimate the rate of deformation-induced mass transfer. It is 18–19 orders of magnitude higher than the rate of conventional thermal diffusion at the processing temperature T_{HPT} = 30°C, while it is close to the diffusivity values at 700–800°C. This is because HPT increases the concentration of lattice defects, which in turn is equivalent to an increase in temperature. A similar combination of accelerated mass transfer during HPT and martensitic (shear) transformation was previously observed in copper-based shape memory alloys, but for the first time studied for the formation of ω-phase in titanium alloys.

DOI: 10.1134/S0021364020100033

Severe plastic deformation (SPD) and, in particular, high-pressure torsion (HPT) can cause various phase transformations in solids [1–7]. Among them are the transformations of crystalline phases into amorphous [8–12], and amorphous ones into crystalline [8, 13, 14]. Severe plastic deformation can also lead to competition between decomposition and the formation of a supersaturated solid solution upon dissolution of particles of the second phase [6, 15–17]. Transformations caused by SPD include transitions between allotropic modifications of substances, and in particular, the formation of the high-pressure ω phase in alloys based on titanium, zirconium, and hafnium [18–25]. Phase transformations during SPD can be both martensitic (shear) ones [26–28] as well as diffusive (with mass transfer) [6, 15, 17, 28–32]. Along with phase transformations, during SPD, microstructure changes that are usual for this process also occur, in particular, grain refinement, as well as hardening by the Hall–Petch mechanism [27]. In the latter case, we are talking about the fact that with a decrease in grain size, many new grain boundaries arise, which impede the movement of dislocations and, thus, increase the strength of the material.

An important feature of SPD is that the material under the influence of external deformation is placed in such geometric conditions that, despite the influence of external forces, it is deformed, but cannot be destroyed [4, 6]. It is clear that the accumulation of lattice defects under the influence of external deformation cannot occur infinitely. This means that relaxation processes begin in the material during SPD, and their rate increases until the processes of formation of defects and their annihilation are equalized. Then, a

stationary state occurs in which the structure parameters and phase composition cease to change with a further increase in deformation. It is interesting to note that these parameters in the stationary state, as it turned out, are almost independent of the initial structure and material properties. In other words, the stationary state in SPD is characterized by the so-called equifinality [33]. This means that the structure and properties of the material in a stationary state are affected by the deformation parameters (pressure, temperature, strain rate), but not by the initial state. At the same time, it is obvious that the path from the initial state to the stationary one will strongly depend on the initial state of the material. The study of the features of this path is the goal of this work.

As an object for research, we chose a Ti–4 wt % Fe alloy. In our recent work, we found that HPT in this alloy causes an almost 100% transition of the β- and α-phases to the high pressure ω-phase [26]. This is due to the fact that, when iron is added to titanium, the β-phase lattice period decreases and the ω-phase lattice period remains almost unchanged. As a result, at 4 wt % Fe, the orientation relationship between the initial β-phase and the ω-phase becomes almost ideal, and the β-phase quickly and easily passes into the ω-phase during HPT. This transformation proceeds by a martensitic (shear) mechanism, without mass transfer. If the iron concentration in titanium is less than or more than four percent, then the volume fraction of the ω-phase after HPT decreases. Moreover, mass transfer occurs during the phase transition $(\alpha + \beta) \rightarrow \omega$, and it does not remain completely martensitic [26]. In this work, we also found that the result of this transformation is almost independent of the initial fraction of the α- and β-phases in the sample [26]; therefore, this object seems to us to be ideal for studying the ways of $(\alpha + \beta) \rightarrow \omega$ transformation and reaching a stationary state with 100% of ω-phase during HPT.

The Ti–4 wt % Fe alloy for our experiments was prepared using induction melting in vacuum (from titanium and iron with a purity of 99.9 wt %) in the form of ingots with a diameter of 10 mm. They were cut into 0.7 mm thick disks by the spark erosion. These disks were sealed in evacuated quartz ampoules with a residual pressure of 4×10^{-4} Pa. Ampoules with samples were annealed in a SUOL resistance furnace at temperatures of 800°C for 100 h and 615°C for 270 h. Points corresponding to annealing temperatures and alloy concentrations of 4 wt % iron, are positioned in the Ti–Fe phase diagram in the αTi + βTi region [34]. After annealing, the samples were quenched in water (the ampoules were broken). After annealing and quenching, the samples were subjected to HPT in a Bridgman anvil cell (W. Klement GmbH, Lang, Austria) at room temperature, pressure of 7 GPa and five revolutions anvil at a speed of 1 rpm. Samples for structural studies were mechanically ground and polished on diamond paste with a grain size down to 1 μm. Samples after HPT were cut out at a distance of 3 mm from the center of the deformed disk. The resulting sections were studied using scanning electron microscopy (SEM) and X-ray microanalysis on a Tescan Vega TS5130 MM instrument equipped with a LINK energy dispersive spectrometer (Oxford Instruments). X-ray diffraction patterns were obtained in Bragg–Brentano geometry on a Philips X'Pert powder diffractometer using Cu $K\alpha$ radiation. The lattice parameter was determined using the Fityk program [35]. Alloy phases were identified by comparison with X'Pert HighScore Panalytical phase database. Transmission electron microscopy (TEM) was performed on a TECNAI G2 FEG super TWIN (200 kV) microscope equipped with an energy dispersive spectrometer (EDAX). Thin-film samples for TEM were made by electro polishing on an Electrolyte D2 device (Struers).

The annealing temperatures of our samples were chosen in the region of α + β of the Ti–Fe phase diagram in such a way that the temperature of 800°C lies near the transus line (being the boundary between the region of α + β and the single-phase β-region in the phase diagram of titanium alloys). Thus, at a temperature of 800°C, in accordance with the phase diagram, the sample should contain almost only the β-phase and a small amount of α-phase. A temperature of 615°C is also in the two-phase α + β region, but it is only slightly higher than the temperature of the eutectoid transformation of the β-phase into a mixture of the α-phase and TiFe intermetallic compound [34].

Figure 1a shows a SEM image of a sample annealed at a temperature of 800°C. The β-phase in this image appears light-gray, and the α-phase looks dark-gray. It is clearly seen that, as expected, the β-phase predominates in the bulk of the sample. In this case, the α-phase is located both in the volume of β-phase grains in the form of small particles, and along the β/β grain boundaries in the form of continuous interlayers or in the form of particle chains. In this case, we are dealing with the phenomenon of the so-called "wetting" of grain boundaries by interlayers of the second solid phase [36–39]. We studied this phenomenon in detail for a number of titanium-based alloys [36, 40–44]; it is observed, as a rule, in the two-phase α + β region of the phase diagram. At high temperature, the α-phase almost completely "wets" all grain boundaries in the β-phase, and as the temperature decreases, the fraction of boundaries in the β-phase completely "wetted" by layers of the α-phase decreases gradually [40–44]. Therefore, in Fig. 1b it is clearly seen that, indeed, that the fraction of the α-phase at the annealing temperature of 615°C is much higher than at the temperature of 800°C. In this case, only individual boundaries between the grains of the β-phase are completely covered by interlayers of the α-phase. At low temperatures, the grain boundaries with the high-

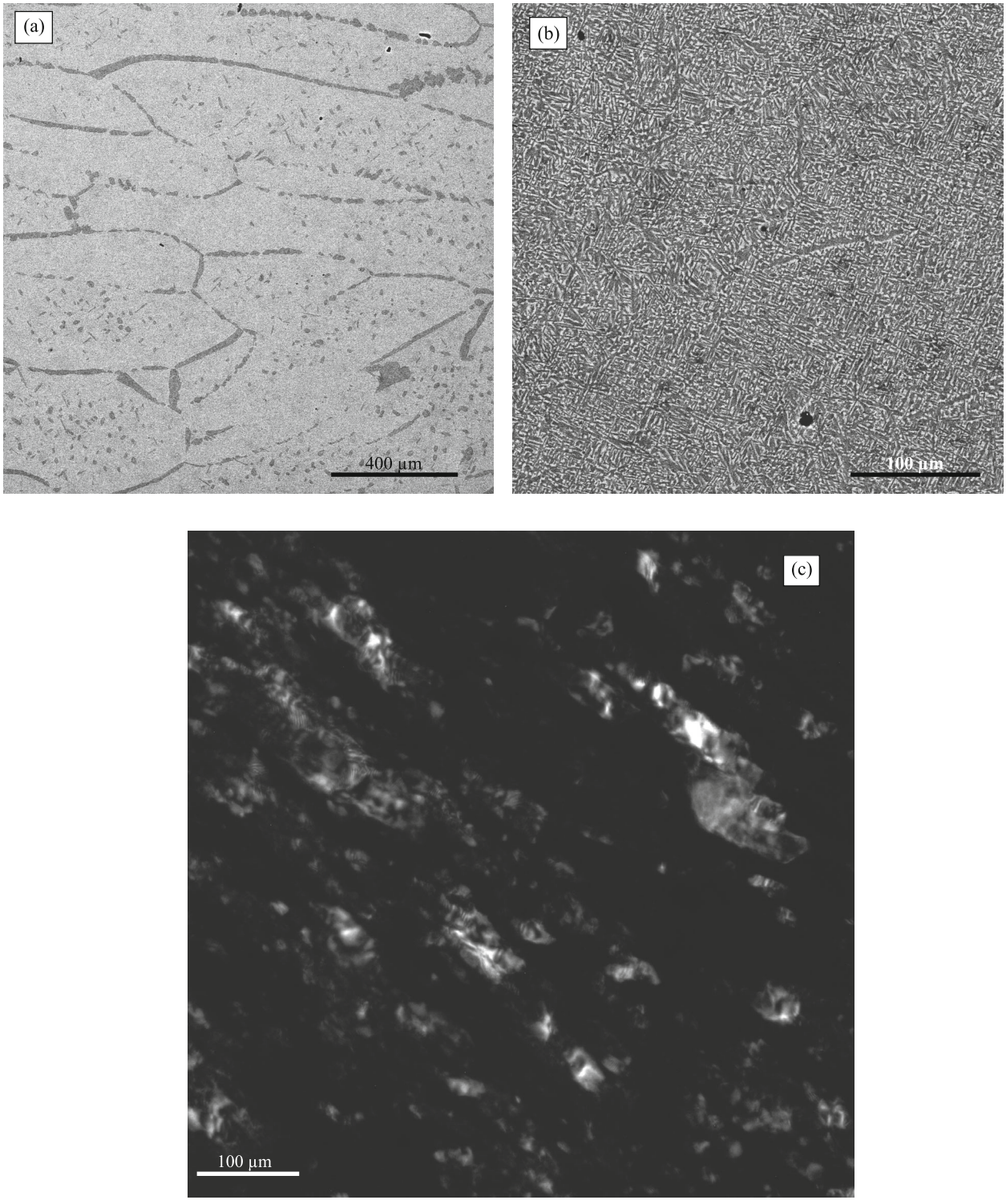

Fig. 1. SEM images of Ti–4 wt % Fe alloy annealed at (a) 800°C, 100 h and (b) 615°C, 270 h. (c) Dark-field TEM image of the same alloy after HPT at five revolutions.

est energy remain completely wetted [45]. Figure 1c shows a dark-field TEM image of the same alloy after HPT at five revolutions. It can be seen that the grains after HPT are not completely equiaxial, but slightly elongated in the direction of deformation, and their size is about 200 nm.

Figure 2 shows a number of X-ray diffraction patterns of the studied alloy after annealing before HPT,

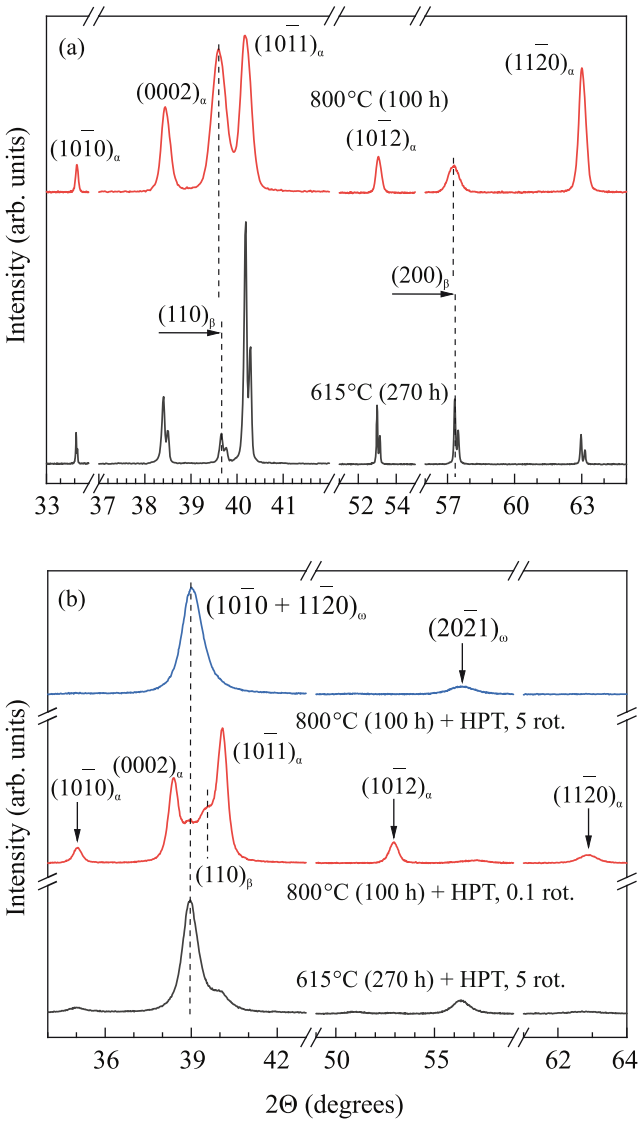

Fig. 2. (Color online) X-ray diffraction patterns of the Ti–4 wt % Fe alloy annealed at 800°C, 100 h and 615°C, 270 h (a) before and (b) after HPT. The top and bottom patterns correspond to HPT at five revolutions. The middle pattern is taken after 0.1 turn on the sample annealed at 800°C, 100 h.

as well as after HPT. The diffraction pattern of the sample after annealing at 800°C (the upper curve in Fig. 2a) really contains peaks of the α- and β-phases, and the fraction of the α-phase in this sample is lower than in the other state studied. Accordingly, after annealing at 615°C, the fractions of the α- and β-phases, as can be expected from the phase diagram, are almost equal (lower curve in Fig. 2a). The dotted line shows the position of the (110) and (200) peaks of the β-phase on the upper and lower curves (the β-phase contains more iron after annealing at 615°C than after annealing at 800°C). After HPT, the X-ray diffraction patterns of the two samples studied (respectively, the upper and lower curves in Fig. 2b) are almost indistinguishable from each other. They mainly contain peaks of the ω-phase with a very small amount of residual α-phase. These results are consistent with previously obtained data [26]. Thus, from the point of view of the content of different allotropic modifications of titanium, the state of the samples after five turns of the HPT plunger is equifinal. In other words, the samples contain only the ω-phase, and their phase composition does not depend on the phase composition before the HPT.

Figure 3 shows the dependences of the torsion torque during HPT on the angle of rotation of the plungers for two samples annealed at 800°C (Fig. 3a) and 615°C (Fig. 3b). The magnitude of the torsion torque is measured directly in the HPT process using a special sensor. Both curves show a rapid increase in torsion torque at the initial stage of deformation (from 0° to about 30°). The initially undeformed sample is hardened due to the grain refinement and increase in the density of dislocations. At high rotation angles (more than 400°), the magnitude of the torsion torque in both samples studied is the same and amounts to ~300 Nm. This corresponds to a stationary state in which, as we saw from Fig. 2, the sample contains almost 100% of high pressure ω-phase. The portions of the curves of the angular dependence of torsion torque between the initial strength increase and the stationary state are different. So in a sample annealed at a temperature of 800°C, the torsion torque increases rapidly and reaches a stationary state already at about 100°. This can be explained by the fact that the initial sample contains a high volume fraction of the β-phase, which, in turn, has an iron concentration closer to the nominal value in the Ti–4 wt % Fe alloy. As shown earlier [26], the HPT of an alloy with 4 wt % Fe in the β-phase leads to a relatively rapid conversion to the ω-Ti phase already in the early stages of deformation. Figure 2b (middle curve) shows the diffraction pattern of the sample annealed at a temperature of 800°C after 0.1 turn of the plunger (rotation angle ~35°). Like the upper curve in Fig. 2a, this pattern contains peaks of the α- and β-phases, but the β-phase has already begun to disappear, and a peak of the ω-phase appears between the $(0002)_\alpha$ and $(110)_\beta$ peaks.

The sample annealed at a temperature of 615°C contains both β- and α-phases. In this case, the α-phase (in accordance with the phase diagram) almost does not contain iron, and the β-phase contains almost 10 wt % Fe (see the shift of β peaks in Fig. 2a) [34]. After HPT, the entire sample contains only ω-Ti with the same concentration of 4 wt % Fe in the whole volume. We can assume that, like in [28], mass transfer precedes the martensitic (shear) transformation. In other words, the iron-poor α-phase should be first mechanically mixed with the iron-rich β-phase. That is why we believe that hardening in the early phase of

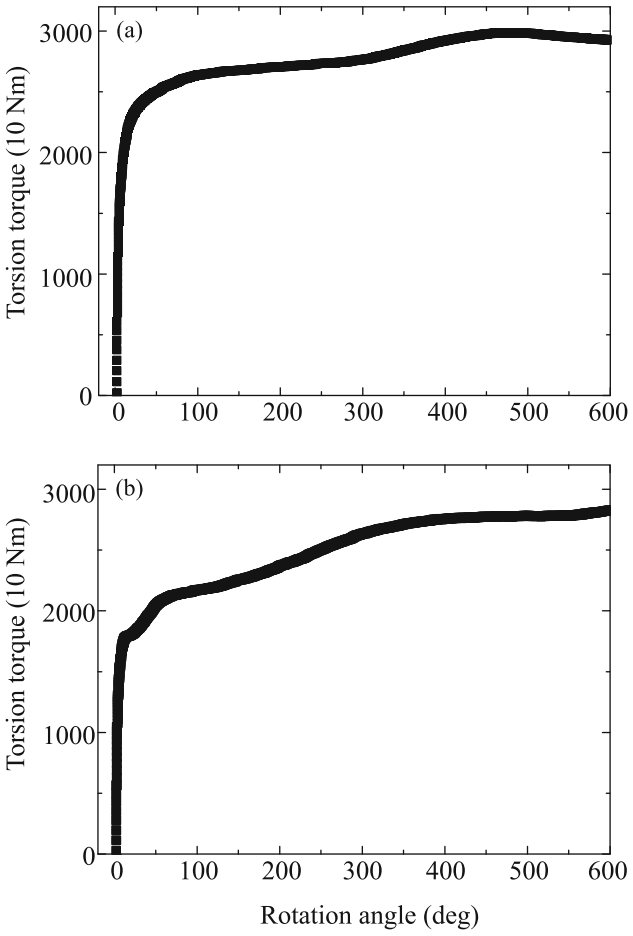

Fig. 3. Torsion torque during HPT versus the angle of rotation of the plunger for the Ti–4 wt % Fe alloy annealed at (a) 800°C, 100 h and (b) 615°C, 270 h.

deformation finishes quickly and a slow and, apparently, two-stage hardening of the alloy begins (Fig. 3b). The first stage takes place from 20° to about 70°. The second stage of alloy hardening occurs in the region from 70° to ~300°. Only after this, the stationary state appears in which the sample contains approximately 100% of the ω-phase.

Thus, during HPT, in addition to diffusionless (and relatively fast) $\alpha \rightarrow \omega$ and $\beta \rightarrow \omega$ transformations, the processes associated with mass transfer also occur. To describe the mass transfer stimulated by HPT in copper and aluminum alloys, we estimated the equivalent diffusion coefficient [6, 15, 17, 29, 30]. Now we perform this assessment for mixing in a titanium alloy. In the initial state (see Fig. 1b), the alloy annealed at 615°C contains the α-phase with almost zero iron content and the β-phase with ~10 wt % Fe. The grain size of the α- and β-phases is approximately $L = 5$ μm (Fig. 1b). After deformation, the sample contains only the ω-phase with 4 wt % Fe (see Fig. 2) and a grain size of approximately 200 nm (Fig. 1c) [26]. The time required to reach this stationary state is approximately $t = 250$ s (see Fig. 3b). Using the simple formula $L = (Dt)^{0.5}$ for mass transfer through volume diffusion, we estimate the volume diffusion coefficient as $D = 10^{-13}$ m^2 s^{-1}. Bulk diffusion of iron in β-titanium occurs at such a rate at ~800°C [46] and in α-titanium at ~700°C [47]. Extrapolation of the data for the volume diffusion of iron in titanium to the temperature of the HPT $T_{HPT} = 30$°C gives the value $D = 10^{-31}$–10^{-32} m^2 s^{-1}. Thus, the $\alpha \rightarrow \beta \rightarrow \omega$ transformation in titanium under the influence of HPT is accompanied by the accelerated mass transfer at a rate 18–19 orders of magnitude higher than the rate of ordinary thermal diffusion at room temperature (i.e., at the HPT temperature T_{HPT}) although high pressure itself significantly reduces the kinetic coefficients of mass transfer [48, 49]. However, it should be noted that in β-titanium (as well as in β-zirconium), the value of D decreases with increasing pressure much more slowly than in metals with face-centered cubic lattice [50–54]. Moreover, for example, iron and chromium diffuse in Ti much faster than the self-diffusion of titanium proceeds [52, 54]. This can be explained by the fact that diffusion in β-Ti occurs not only through vacancies, but also through interstices, and the crowdion mechanism is possible as well [50, 51, 53, 55]. The variety of diffusion mechanisms is manifested in the significant nonlinearity of the Arrhenius dependences for D [46, 47, 50–52, 54, 55]. A similar superposition of two or several "barrier" diffusion mechanisms can lead to various artifacts, such as unphysically high activation energies or even a negative activation volume [56–60].

We observed this phenomenon earlier in the case of HPT-induced competition between the decomposition of a solid solution and the dissolution of particles in copper alloys [6, 17, 29, 30]. As before, we can attribute to the HPT-induced mass transfer some effective temperature $T_{eff} = 700$–800°C [6, 17, 29, 30]. Apparently, this phenomenon is explained by an increased concentration of defects (in particular, vacancies) during high-pressure analysis, and it, in turn, is equivalent to an increase in temperature from T_{HPT} to T_{eff}. In fact, of course, during HPT, a real increase in temperature or acceleration of diffusion does not occur [3, 5, 7, 21, 28, 29]. In HPT, mass transfer occurs over long distances, and on scales from nanometers to millimeters. Moreover, in fact, a huge number of defects of various types are born (and disappear). So, for example, during HPT, the amorphization of a number of alloys is often observed, which does not occur at all when they are heated [8, 12]. As a result, the final picture of processes during HPT is similar to that observed with increasing temperature [61–64].

FUNDING

This work was partially carried out within the framework of the state task of the Institute of Solid State Physics and the Chernogolovka Scientific Center of the Russian Academy of Sciences with the support of the Scientific Facility Center at the Institute of Solid State Physics, as well as with the financial assistance of the Russian Foundation for Basic Research (project nos. 18-33-00473 and 19-58-06002) and the German National Research Society (grant nos. RA 1050/20-1, IV 98/5-1, HA 1344/32-1, FA 999/1-1).

REFERENCES

1. S. K. Pabi, J. Joardar, and B. S. Murty, Proc. Indian Nat.Sci. Acad. A **67**, 1 (2001).
2. X. Sauvage, A. Chbihi, and X. Quelennec, J. Phys.: Conf. Ser. **240**, 012003 (2010).
3. V. I. Levitas and O. M. Zarechnyy, Phys. Rev. B **82**, 174123 (2010).
4. B. B. Straumal, A. R. Kilmametov, Yu. Ivanisenko, A. A. Mazilkin, O. A. Kogtenkova, L. Kurmanaeva, A. Korneva, P. Zieba, and B. Baretzky, Int. J. Mater. Res. **106**, 657 (2015).
5. M. Javanbakht and V. I. Levitas, Phys. Rev. B **94**, 214104 (2016).
6. B. B. Straumal, A. R. Kilmametov, A. Korneva, A. A. Mazilkin, P. B. Straumal, P. Zięba, and B. Baretzky, J. Alloys Compd. **707**, 20 (2017).
7. V. I. Levitas, Mater. Trans. **60**, 1294 (2019).
8. V. I. Levitas, Phys. Rev. Lett. **95**, 075701 (2005).
9. S. D. Prokoshkin, I. Yu. Khmelevskaya, S. V. Dobatkin, I. B. Trubitsyna, E. V. Tatyanin, V. V. Stolyarov, and E. A. Prokofiev, Acta Mater. **53**, 2703 (2005).
10. X. Sauvage, L. Renaud, B. Deconihout, D. Blavette, D. H. Ping, and K. Hono, Acta. Mater. **49**, 389 (2001).
11. A. A. Mazilkin, G. E. Abrosimova, S. G. Protasova, B. B. Straumal, G. Schütz, S. V. Dobatkin, and A. S. Bakai, J. Mater. Sci. **46**, 4336 (2011).
12. V. I. Levitas, Y. Ma, E. Selvi, J. Wu, and J. A. Patten, Phys. Rev. B **85**, 054114 (2012).
13. A. M. Glezer, M. R. Plotnikova, A. V. Shalimova, and S. V. Dobatkin, Bull. Russ. Acad. Sci.: Phys. **73**, 1233 (2009).
14. S. Hobor, Á. Revész, A. P. Zhilyaev, and Zs. Kovács, Rev. Adv. Mater. Sci. **18**, 590 (2008).
15. B. B. Straumal, B. Baretzky, A. A. Mazilkin, F. Phillipp, O. A. Kogtenkova, M. N. Volkov, and R. Z. Valiev, Acta Mater. **52**, 4469 (2004).
16. B. B. Straumal, S. G. Protasova, A. A. Mazilkin, E. Rabkin, D. Goll, G. Schütz, B. Baretzky, and R. Valiev, J. Mater. Sci. **47**, 360 (2012).
17. B. Straumal, A. R. Kilmametov, Yu. O. Kucheev, L. Kurmanaeva, Yu. Ivanisenko, B. Baretzky, A. Korneva, P. Zięba, and D. A. Molodov, Mater. Lett. **118**, 111 (2014).
18. B. B. Straumal, A. A. Mazilkin, B. Baretzky, E. Rabkin, and R. Z. Valiev, Mater. Trans. **53**, 63 (2012).
19. Y. Ivanisenko, I. MacLaren, X. Sauvage, R. Z. Valiev, and H.-J. Fecht, Acta Mater. **54**, 1659 (2006).
20. M. T. Pérez-Prado and A. P. Zhilyaev, Phys. Rev. Lett. **102**, 175504 (2009).
21. B. Feng and V. I. Levitas, Mater. Sci. Eng. A **680**, 130 (2017).
22. K. Edalati, E. Matsubara, and Z. Horita, Metall. Mater. Trans. A **40**, 2079 (2009).
23. B. Feng, V. I. Levitas, and M. Kamrani, Mater. Sci. Eng. A **731**, 623 (2018).
24. Y. Ivanisenko, A. Kilmametov, H. Roesner, and R. Valiev, Int. J. Mater. Res. **99**, 36 (2008).
25. B. Feng, V. I. Levitas, and W. Li, Int. J. Plast. **113**, 236 (2019).
26. A. Kilmametov, Yu. Ivanisenko, A. A. Mazilkin, B. B. Straumal, A. S. Gornakova, O. B. Fabrichnaya, M. J. Kriegel, D. Rafaja, and H. Hahn, Acta Mater. **144**, 337 (2018).
27. A. Mazilkin, B. Straumal, A. Kilmametov, P. Straumal, and B. Baretzky, Mater. Trans. **60**, 1489 (2019).
28. B. B. Straumal, A. R. Kilmametov, G. A. López, I. Lopez-Ferreño, M. L. No, J. San Juan, H. Hahn, and B. Baretzky, Acta Mater. **125**, 274 (2017).
29. B. B. Straumal, V. Pontikis, A. R. Kilmametov, A. A. Mazilkin, S. V. Dobatkin, and B. Baretzky, Acta Mater. **122**, 60 (2017).
30. B. B. Straumal, A. R. Kilmametov, I. A. Mazilkin, A. Korneva, P. Zięba, and B. Baretzky, JETP Lett. **110**, 624 (2019).
31. B. B. Straumal, A. R. Kilmametov, Yu. O. Kucheev, K. I. Kolesnikova, A. Korneva, P. Zięba, and B. Baretzky, JETP Lett. **100**, 376 (2014).
32. B. B. Straumal, A. R. Kilmametov, I. A. Mazilkin, A. Korneva, P. Zięba, and B. Baretzky, JETP Lett. **110**, 624 (2019).
33. L. von Bertalanffy, Science (Washington, DC, U. S.) **111**, 23 (1950).
34. *Binary Alloy Phase Diagrams,* Ed. by T. B. Massalski, 2nd ed. (ASM Int., Materials Park, OH, 1990).
35. M. Wojdyr, J. Appl. Crystallogr. **43**, 1126 (2010).
36. B. B. Straumal, A. S. Gornakova, Y. O. Kucheev, B. Baretzky, and A. N. Nekrasov, J. Mater. Eng. Perfom. **21**, 721 (2012).
37. B. B. Straumal, B. S. Bokstein, A. B. Straumal, and A. L. Petelin, JETP Lett. **88**, 537 (2008).
38. O. A. Kogtenkova, B. B. Straumal, S. G. Protasova, A. S. Gornakova, P. Zięba, and T. Czeppe, JETP Lett. **96**, 380 (2012)].
39. B. B. Straumal, O. A. Kogtenkova, K. I. Kolesnikova, A. B. Straumal, M. F. Bulatov, and A. N. Nekrasov, JETP Lett. **100**, 535 (2014).
40. B. B. Straumal, A. R. Kilmametov, Yu. Ivanisenko, A. S. Gornakova, A. A. Mazilkin, M. J. Kriegel, O. B. Fabrichnaya, B. Baretzky, and H. Hahn, Adv. Eng. Mater. **17**, 1835 (2015).
41. A. S. Gornakova, S. I. Prokofiev, B. B. Straumal, and K. I. Kolesnikova, Russ. J. Non-Ferr. Met. **57**, 703 (2016).
42. A. S. Gornakova, B. B. Straumal, A. N. Nekrasov, A. Kilmametov, and N. S. Afonikova, J. Mater. Eng. Perform. **27**, 4989 (2018).

43. A. S. Gornakova, A. B. Straumal, I. I. Khodos, I. B. Gnesin, A. A. Mazilkin, N. S. Afonikova, and B. B. Straumal, J. Appl. Phys. **125**, 082522 (2019).
44. A. S. Gornakova, B. B. Straumal, and S. I. Prokofiev, Adv. Eng. Mater. **20**, 1800510 (2018).
45. B. B. Straumal, P. V. Protsenko, A. B. Straumal, A. O. Rodin, Yu. O. Kucheev, A. M. Gusak, and V. A. Murashov, JETP Lett. **96**, 582 (2012).
46. G. B. Gibbs, D. Graham, and D. H. Tomlin, Philos. Mag. **8**, 1269 (1963).
47. H. Nakajima, M. Koiwa, and S. Ono, Scr. Metall. **17**, 1431 (1983).
48. B. B. Straumal, L. M. Klinger, and L. S. Shvindlerman, Scr. Metall. **17**, 275 (1983).
49. D. A. Molodov, B. B. Straumal, and L. S. Shvindlerman, Scr. Metall. **18**, 207 (1984).
50. H. Araki, Y. Minamino, T. Yamane, Y. Shirai, and Y. Miyamoto, Defect Dif. Forum **143–147**, 125 (1997).
51. H. Araki, Y. Minamino, T. Yamane, S. Saji, S. Ogino, and Y. Miyamoto, J. Jpn. Inst. Met. Mater. **57**, 501 (1993).
52. H. Araki, Y. Shirai, T. Yamane, and Y. Miyamoto, Rev. High Press. Sci. Technol. **7**, 676 (1998).
53. P. Knorr, J. Jun, W. Lojkowski, and Chr. Herzig, Phys. Rev. B **57**, 334 (1998).
54. H. Araki, T. Yaman, T. Nakatuka, and Y. Minamino, Z. Metallkd. **97**, 22 (2006).
55. U. Köhler and Ch. Herzig, Phys. Status Solidi B **144**, 243 (1987).
56. B. Straumal, E. Rabkin, W. Gust, and B. Predel, Acta Metall. Mater. **43**, 1817 (1995).
57. E. Rabkin, B. Straumal, V. Semenov, W. Gust, and B. Predel, Acta Metall. Mater. **43**, 3075 (1995).
58. R. F. Peart, Phys. Status Solidi **20**, 545 (1967).
59. S. D. Gertsriken and M. P. Pryanishnikov, Fiz. Met. Metalloved. **2**, 297 (1960).
60. R. N. Jeffery, Phys. Rev. B **3**, 4044 (1971).
61. T. Kim, G. Ouyang, J. D. Poplawsky, M. J. Kramer, V. I. Levitas, J. Cui, and L. Zhou, J. Alloys Compd. **808**, 151743 (2019).
62. M. Kamrani, V. I. Levitas, and B. Feng, Mater. Sci. Eng. A **705**, 219 (2017).
63. V. I. Levitas and A. M. Roy, Phys. Rev. B **91**, 174109 (2015).
64. V. I. Levitas, Int. J. Plast. **106**, 164 (2018).